Materials Today Bio 8 (2020) 100074

Contents lists available at ScienceDirect

Materials Today Bio

journal homepage: www.journals.elsevier.com/materials-today-bio

An open-source handheld extruder loaded with pore-forming bioink for *in situ* wound dressing

G. Ying [a,c], J. Manríquez [a,c], D. Wu [a,c], J. Zhang [a], N. Jiang [b], S. Maharjan [a], D.H. Hernández Medina [a], Y.S. Zhang [a,*]

[a] Division of Engineering of Medicine, Department of Medicine, Brigham and Women's Hospital, Harvard Medical School, Cambridge, MA, 02139, USA
[b] School of Engineering and Applied Sciences, Harvard University, Cambridge, MA, 02138, USA

ARTICLE INFO

Keywords:
Gelatin methacryloyl (GelMA)
Polyethylene oxide (PEO)
Porous
Bioprinting
Intraoperative
Minimally invasive

ABSTRACT

The increasing demand in rapid wound dressing and healing has promoted the development of intraoperative strategies, such as intraoperative bioprinting, which allows deposition of bioinks directly at the injury sites to conform to their specific shapes and structures. Although successes have been achieved to varying degrees, either the instrumentation remains complex and high-cost or the bioink is insufficient for desired cellular activities. Here, we report the development of a cost-effective, open-source handheld bioprinter featuring an ergonomic design, which was entirely portable powered by a battery pack. We further integrated an aqueous two-phase emulsion bioink based on gelatin methacryloyl with the handheld system, enabling convenient shape-controlled in situ bioprinting. The unique pore-forming property of the emulsion bioink facilitated liquid and oxygen transport as well as cellular proliferation and spreading, with an additional ability of good elasticity to withstand repeated mechanical compressions. These advantages of our pore-forming bioink-loaded handheld bioprinter are believed to pave a new avenue for effective wound dressing potentially in a personalized manner down the future.

1. Introduction

The three-dimensional (3D) bioprinting technologies have been rapidly advancing over the past decade as an outcome of the increasing demand for functional human tissues and organs, used toward either regenerative medicine or drug development [1]. Indeed, immense potential of this class of enabling technologies has been demonstrated over the years [2–6]. Nevertheless, the tissue defects usually feature curved surfaces or even more intricate geometries in a wound-specific manner. To this end, the conventional 3D bioprinting strategies become oftentimes insufficient as they typically have to be used for fabricating biological tissues outside of the body followed by in vivo transplantation, where the mismatch of the shapes may be further worsened by the possible deformation of the local tissues, thus restricting their range of applications.

To address this dilemma, in situ bioprinting, or also termed as intraoperative bioprinting, has received significant attention lately to facilitate repair and reconstruction of defective tissues by directly producing prohealing structures at the defect sites in a clinical setting [7,8]. In realizing such a goal, three-axis movable bioprinting units have been accordingly designed, where the in situ bioprinting processes are controlled by dedicated software to achieve precise spatial deposition of the dressing biomaterials [9–11]. This approach is referred to by us as the robotic arm approach, which has interestingly been more recently extended to a few other variations enabled by light-based bioprinting, requiring only single-axis movements [12,13].

Another in situ bioprinting approach relies on the adoption of the handheld bioprinting systems. In this case, neither defect scanning nor computer-aided path-planning is needed, and an operator can simply hold the bioprinter to directly deposit the bioink on-site through moving the hand. This strategy provides a decent degree of freedom to the clinician using the device, allowing rapid adjustments to the wound shape/structure when using the bioprinting device as well as any potential patient movement during the operation, which cannot be conveniently accommodated by the robotic arm method. Several investigational studies have shown the potential of handheld bioprinting in intraoperative wound-dressing applications, such as healing of the skin [14,15], the muscle [16], and the bone [17], among others.

* Corresponding author.
E-mail address: yszhang@research.bwh.harvard.edu (Y.S. Zhang).
[c] These authors contributed equally to this work.

https://doi.org/10.1016/j.mtbio.2020.100074
Received 5 July 2020; Received in revised form 10 August 2020; Accepted 11 August 2020
Available online 21 August 2020

On the other hand, bioinks are also a key component in ensuring successful bioprinting, as they should not only allow proper structural fidelity during and after bioprinting but also support the survival and functions of the embedded cells on subsequent culture or implantation [18,19]. Among the various bioinks, those that facilitate nutrient transport, cellular spreading, proliferation, and migration are of particular interest. These bioinks usually lead to the formation of interconnected pores in the range of a few tens to hundreds of micrometers, which can be readily achieved by incorporating a sacrificial component within a non-removable, primary bioink matrix. For example, Shao et al. recently reported synchronous 3D extrusion bioprinting of constructs containing nutrient networks by side-by-side depositing gelatin methacryloyl (GelMA) and gelatin bioinks using a dual-channel printhead [20]. After the photocrosslinking of the GelMA component, the gelatin bioinks could be selectively removed to form the networks for nutrient transport and cellular activities. While efficient in desktop bioprinting, this method is hindered by the need for reduced temperature during bioprinting to secure structural fidelity of the gelatin component due to the miscibility of GelMA and gelatin, and the control over the pore size toward a smaller scale was limited. Instead, we have also recently developed a two-phase aqueous emulsion bioink formulation based on the mixture of GelMA and polyethylene oxide (PEO) solutions [21]. This bioink is unique because the immiscibility of the two phases of GelMA and PEO, despite that they are both aqueous, has significantly expanded its potential utility in various scenarios—the biocompatibility of both components allows cell encapsulation in the GelMA phase during bioprinting; the bioink does not have to be used in the gel phase because of the phase separation; and the pore size can be conveniently designed across a wide range by tuning the emulsion parameters. The utility of such a pore-forming bioink toward in situ wound dressing has also not been previously demonstrated.

Here, we demonstrated the combined advantages of an ergonomic handheld bioprinter and a pore-forming bioink for promoting our capacity in situ bioprinting (Fig. 1). We first designed a low-cost handheld bioprinter that featured an ergonomic body for holding in hand, a set of switches for controlling the extrusion process, and an array of embedded ultraviolet (UV) light-emitting diodes (LEDs) for photocrosslinking, all operated using a battery pack without needing the external power source. All the components of this handheld bioprinter, including the STL files for the 3D-printed encasements, the mechanotronic units, and the controller software, are made open-source (Supplementary data). We further loaded our pore-forming GelMA/PEO aqueous two-phase emulsion bioink into the handheld bioprinter and validated the potential of the device toward in situ bioprinting in vitro and directly on ex vivo tissues. The viability and spreading of the embedded cells, including fibroblasts and endothelial cells following in situ bioprinting, were finally characterized.

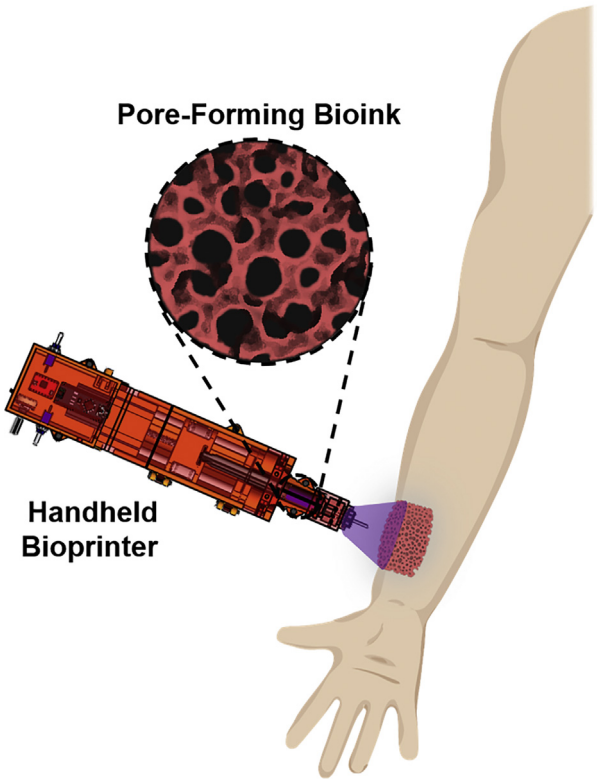

Fig. 1. Schematic diagram illustrating the concept of using a low-cost, open-source, and ergonomic handheld bioprinter for in situ wound dressing using a pore-forming bioink formulation.

2. Materials and methods

2.1. Design of the handheld bioprinter

The overall design considerations of our handheld bioprinter emphasized portability, maneuverability, and low cost. The entire device was roughly $121 in cost (Table S1), which is made completely open-source for all its hardware and software packages (Supplementary data).

2.1.1. Hardware

The handheld bioprinting system contained a motorized extrusion system, a bioink cartridge, a nozzle, and a photocuring unit, operated by a portable battery (Fig. 2A and B). All these parts were assembled in the plastic encasement pieces, which were printed out of red acrylonitrile butadiene styrene (ABS) filaments (1.75-mm diameter, Hatchbox, USA) using a commercial FlashForge Creator Pro 3D Printer (FlashForge, USA). The STL files are supplied in Supplementary data 1.

The motorized extrusion system was based on a stepper motor to allow the extrusion of the bioink in a cartridge (in this work, a 5-mL syringe was used) at a constant speed, which could be adjusted to meet the requirements of the bioinks. There was a potentiometer to allow this change of the motor rotation speed that translated into linear motions of the syringe plunger, as well as two switches to control the direction and the turning ON/OFF of the stepper motor, respectively. Two main operation modes were built in: in the first one, a mobile part could travel forward and push the plunger of the syringe to extrude; and in the second one, it could instead be retracted at a much faster speed to position a new syringe.

The photocuring unit was a removable part that could be plugged into the device, which contained an array of five UV LEDs with the purpose of photocrosslinking the bioink in situ. There was also a switch to control the turning ON/OFF of the LEDs.

While we designed our handheld bioprinter to be driven by a battery pack to make it completely portable, it might be run with electrical power obtained from a common outlet as well when needed. The device had a self-regulating mechanism made possible by the restriction of the current limit of the motor driver, to prevent further rotation once it reached its end.

2.1.2. Electronics and software

The handheld bioprinter was designed to enable control of both speed and direction of the stepper motor (NEMA11) and the photocuring unit, to achieve maximum extruding precision at high levels of torque. The controller system was based on the connection of an Easy driver (A4988 or TMC2100) operated by an Arduino Nano to the stepper motor and the array of 5 UV LEDs (Fig. 2C and D).

A power supply of 12-V direct current (DC) with a minimum current delivery of 2 A was used both to power the Easy Driver (VMOT pin) and the 7805 voltage converter. This power could be provided by either a DC adapter plugged to a common alternating current outlet, although we

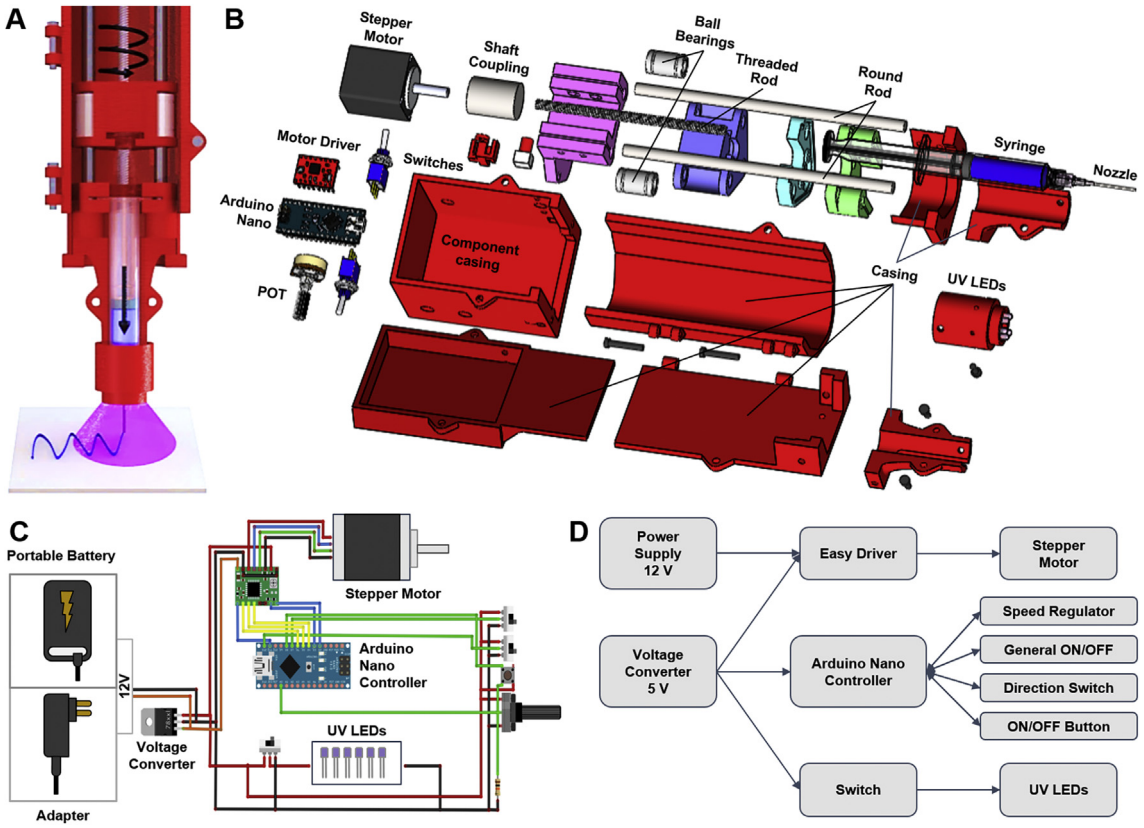

Fig. 2. (A) Schematic showing the design of the handheld bioprinter. (B) Exploded schematic view showing the components and assembly of the handheld bioprinter. (C) Schematic showing the design of the controller system of the handheld bioprinter. (D) Diagram showing the operational principle of the handheld bioprinter.

adopted a battery pack (a model safely protected for overcharge, over discharge, and short circuit) to achieve full portability. To allow convenient exchange between these two power sources, a power jack was inserted in the main outer wire of the device.

A voltage converter was used to deliver a 5-V main power supply for the Easy Driver (Vdd pin), Arduino Nano (5-V V_{in} pin), the photocuring unit (array of 5 UV LEDs; 365 nm, 4.2 V, 20 mA), as well as the signal components including the single pole double throw (SPDT) switches, the nailed button, and the 10-kΩ potentiometer. The potentiometer made it possible to tune the motor rotation speed in the range of 7–31°/s, which translated to a linear moving speed of the piston at 0.015–0.068 mm/s. This feature made it suited for a wide selection of bioinks of variable viscosities and range of resolutions required.

Before the mount of the Easy Driver, the V_{ref} pin must be adjusted to set the current limit (in this case 0.6 A), which would serve as a way both of preventing overheating the motor and also providing a self-regulating mechanism to block further rotation of the mobile part when the stroke end position was reached. The connections of the driver are represented in Fig. 2D. To connect the motor to the driver, the two coils must be identified and wired accordingly.

The Arduino code used in this work is provided (Supplementary data 2). It consisted of a while loop with cases to switch among four modes: standing by, moving forward with the desired variable speed, moving backward quickly to return to the initial position, and a quick reverse mode to release accumulated pressure. To achieve this, different microstepping configurations, up to 1/16 step, were used.

The photocuring unit consisted of an array of five UV LEDs in a parallel connection, controlled by an SPDT switch. This removable part could be connected through a jack plug located in an outer wire of the device. Each LED had a power of 60 mW.

It is further worth mentioning the following tips assembling and operating the handheld bioprinter described herein: i) The Arduino Nano should be programed before inserting it in the circuit to avoid short circuit occasioned by powering it from two voltage sources; ii) The motor should not be disconnected from the driver when it is enabled and functioning; iii) The driver, controller, and power sources should be properly common-grounded; and iv) It is ideal to use a printed circuit board (PCB) to facilitate the wiring and use pin-holders to protect the driver and controller. The designs of the PCB boards are also supplied in Supplementary data 3.

2.2. Preparation of the two-phase aqueous emulsion bioink

The pore-forming GelMA-based bioink was prepared through mixing two immiscible aqueous phases [21]. The first aqueous phase was the GelMA pre-gel solution, which is photocrosslinkable. The other aqueous phase was the PEO solution, which does not photocrosslink and subsequently forms a pore structure on removal. To prepare the GelMA solution, GelMA (high degree of methacryloyl substitution; conversion of amine groups: ~84%) was synthesized according to our previously reported protocol [21–23], and prepared at a final concentration of 10 wt% in phosphate-buffered saline (PBS; Thermo Fisher, USA) containing 0.5 wt% lithium phenyl-2,4,6-trimethylbenzoylphosphinate (LAP; Allevi, USA). PEO used had a molecular weight of 300,000 Da (Sigma-Aldrich, USA), and was prepared at a final concentration of 1.6 wt% in PBS. The pore-forming bioink was prepared by dispersing the PEO solution in the GelMA pre-gel solution followed by vigorous mixing.

NIH/3T3 fibroblasts (ATCC, USA) were maintained in Dulbecco's modified Eagle's medium (DMEM) supplemented with 10 vol% fetal bovine serum and 1 vol% penicillin–streptomycin (all from Thermo Fisher), and human umbilical vein endothelial cells (Angio-Proteomie, USA) in endothelial growth medium (EGM, Lonza, USA), with both in a humidified incubator with 5 vol% CO_2 at 37 °C. The cells were passaged approximately twice per week and the culture medium was exchanged

every 2 days. In cases where the cells were encapsulated in the pore-forming bioink, the cells were trypsinized and resuspended in the GelMA phase before forming the GelMA/PEO emulsion. The final cell concentration was adjusted to be approximately 5×10^6 mL^{-1}.

2.3. Bioprinting

The bioink (2 mL) was loaded into a syringe (5 mL), followed by cooling at 4 °C for 20 min to reduce its temperature to approximately 15 °C to achieve the viscosity optimal for extrusion. It should be noted that this procedure has been shown not to affect cell viabilities as we previously demonstrated [21,24]. Then, the syringe was assembled into the handheld bioprinter. Through turning on the ON/OFF switch, the bioprinting could be initiated and controlled on demand. The extruding speed (i.e. the motor rotation rate) was adjusted to fit the bioprinting speed (i.e. the hand moving speed at 200–1200 mm/min). Besides, the LEDs were turned on to enable photocrosslinking of the bioink during the bioprinting process. The suitable viscosity and the continuous UV illumination ensured proper deposition of the bioink and photocrosslinking of the GelMA phase forming a hydrogel after bioprinting. When necessary, the bioink was labeled with fluorescence to aid visualization.

Also note that this cooling step is not stringently required; in comparison, the liquid bioink may be directly used to automatically fill the wound area after extrusion and before photocrosslinking. Nevertheless, we found improving the viscosity of our bioink through cooling to promote the printing fidelity in this particular scenario.

Significantly, as in our study, the hand movement was involved during the extrusion of the bioink when filling the wounds, we still termed our device as 'handheld bioprinter' and this process as 'handheld bioprinting' due to the shape-control element. However, if only a liquid bioink is used without any need for hand movement during dressing, a terminology of 'handheld extruder/extrusion' might be more suitable then.

2.4. Biological characterizations

To characterize the viability, proliferation, and spreading of fibroblasts in the hand-bioprinted hydrogels, live/dead assay and prestoblue assay (ThermoFisher) were carried out according to manufacturer's instructions. To assess cell spreading, the hand-bioprinted cell-laden hydrogel constructs were fixed with 3.7 vol% paraformaldehyde (Sigma-Aldrich) in PBS and subsequently permeabilized with 0.3 vol% Triton-X 100 (Sigma-Aldrich) in 1 w/v% bovine serum albumin (Sigma-Aldrich). The fixed constructs (laden with fibroblasts or HUVECs) were stained for F-actin and nuclei with Alexa 488-phalloidin and propidium iodide (Thermo Fisher), respectively. The hydrogels were observed under a fluorescence microscope (Nikon Eclipse Ti–S, Japan) or a confocal laser scanning fluorescence microscope (Leica TCS SP5, Germany). Quantification analyses were carried out using ImageJ (National Institutes of Health, USA).

2.5. Statistical analysis

Statistical analyses were carried out using unpaired *t*-tests for comparison between two groups of samples. The statistical significances were determined at $^*p<0.05$, $^{**}p<0.01$, and $^{***}p<0.001$.

3. Results and discussion

Several types of pore-forming bioinks have been reported. In an early demonstration, a bioink composed of GelMA and gelatin allowed

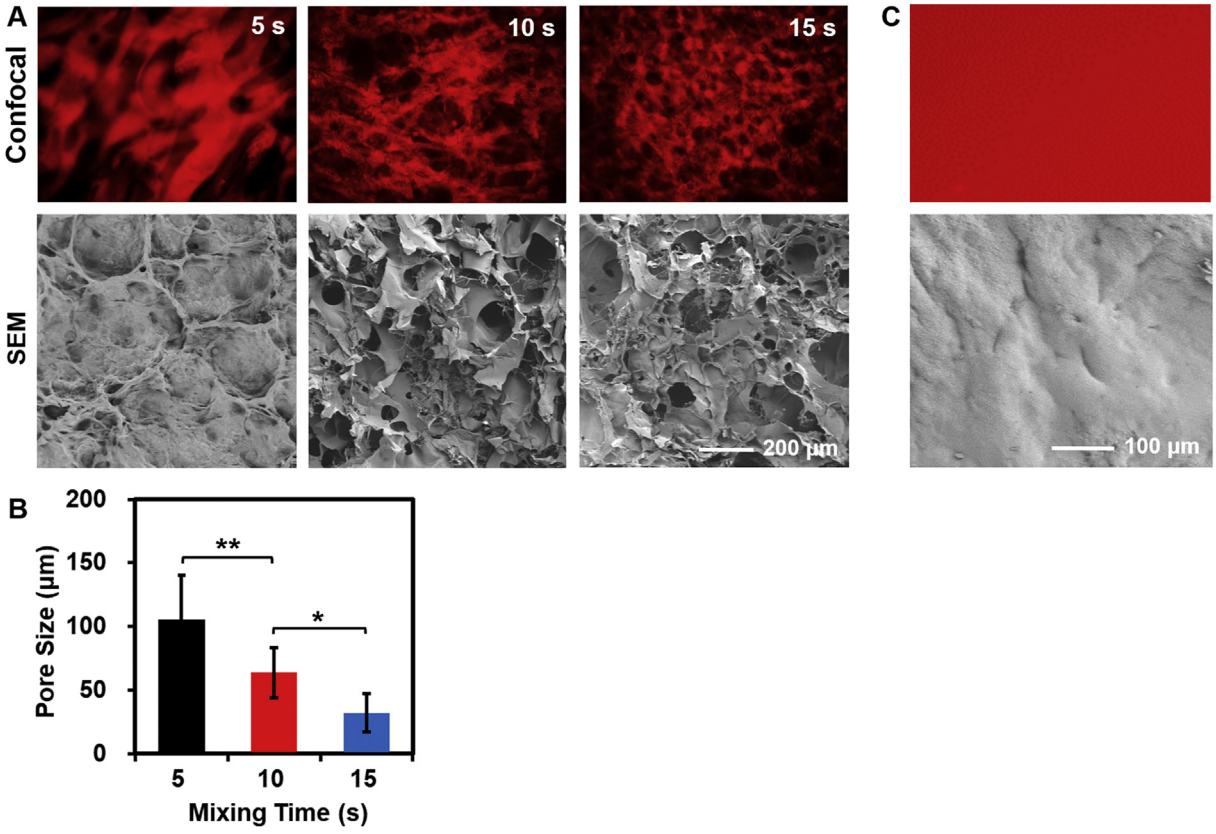

Fig. 3. (A) Confocal fluorescence images and SEM images of the GelMA porous hydrogels formed by the GelMA/PEO aqueous two-phase emulsion bioinks made by mixing the two solutions for different times. The GelMA solution was 10 wt% while PEO 1.6 wt%, with a volume ratio at 1:1. (B) Quantification of the pore sizes of the resulting GelMA porous hydrogels. (C) Confocal fluorescence and SEM images of a standard GelMA hydrogel formed by bioink without the PEO emulsion droplets. $^*p<0.05$, $^{**}p<0.01$.

convenient extrusion bioprinting, where the subsequent leaching of the non-crosslinked gelatin component led to improved cellular activities [25]. Nevertheless, such an increase in the pore size was only limited to that of the hydrogel meshes, which were still small typically in the range of nanometers. More recently, this technique was expanded to the use of a dual-nozzle printhead to extrude GelMA and gelatin filaments side-by-side, obtaining tissue-like constructs possessing interconnected networks limited to larger channel sizes [20]. Albeit effective, the requirement of precise temperature control to maintain shape integrity of the porogen, gelatin, in fact in both of these two examples, made them less attractive in certain application scenarios such as intraoperative bioprinting.

Another method via templating against Pluronic micelles was also developed [26], which however, was hampered by the fact that only relatively small pore sizes of approximately 8 μm could be attained. It has been reported almost unanimously that the porosity of the engineered scaffolds is crucial to allow diffusion of oxygen and nutrients, along with various growth factors for survivability and normal functions of embedded cells until neovascularization is achieved [27,28]. Furthermore, the pore size of scaffolds could play a role in determining the cell/tissue behaviors such as their spreading, proliferation, and migration [29–35].

One commonly used strategy for fabricating porous scaffolds with easily adjustable pore sizes is emulsion [36–38]. Emulsion is produced by mixing two immiscible fluids, usually an aqueous phase and an oil phase, where one forms droplets within the other. This concept has also been applied to 3D printing of porous scaffolds [39,40]. However, the key pitfall lies in that in most cases, the oil phase involves one or more types of organic solvents that are non-compatible with biological cells, meaning that the cells can only be seeded after scaffold fabrication thus significantly reducing the potential applications.

Interestingly, it was found that emulsions do not necessarily have to form between a water phase and an oil phase. Instead, they may as well be formed between two aqueous phases, i.e. the aqueous two-phase

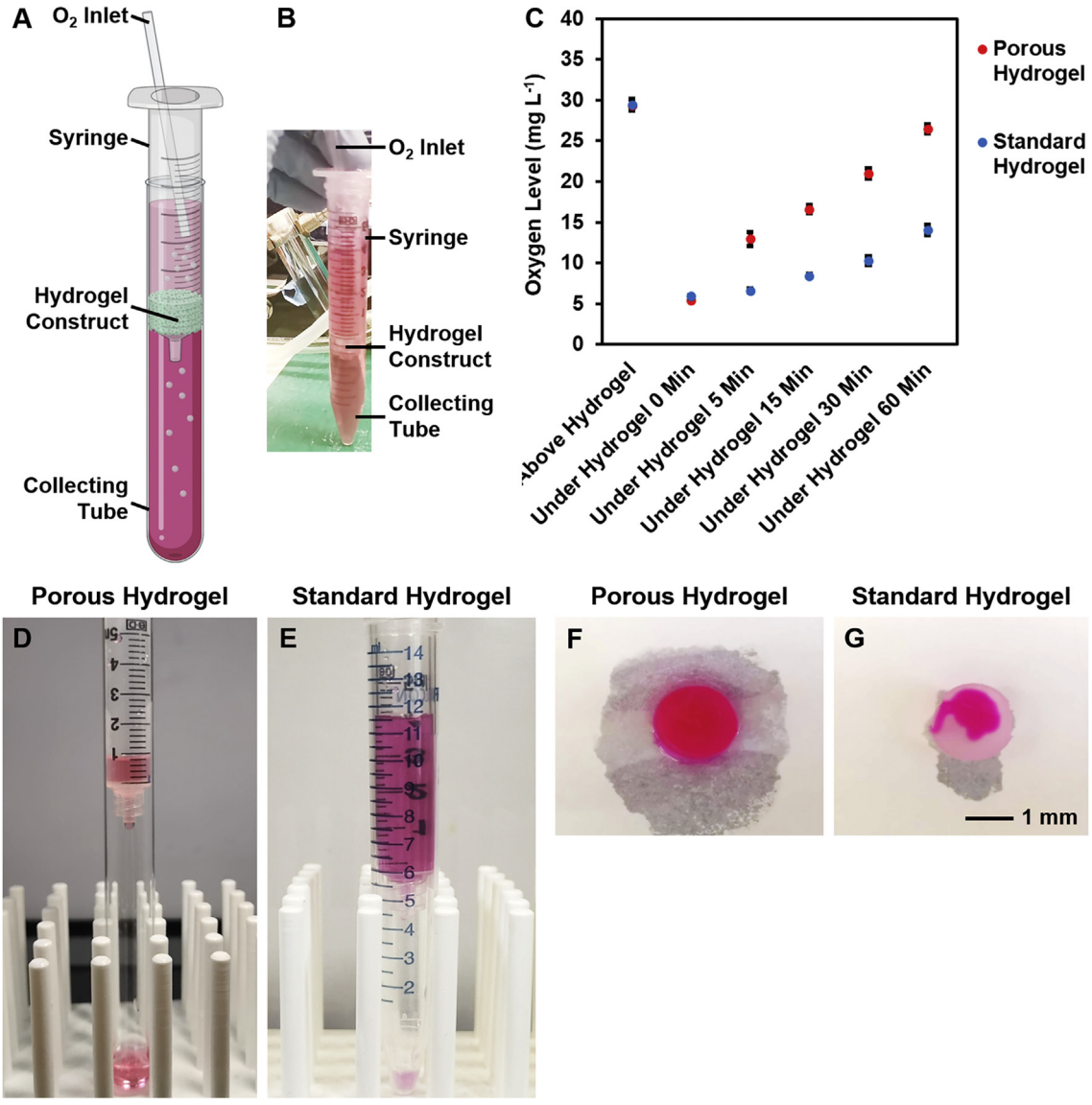

Fig. 4. (A, B) Schematic and photograph showing the setup for measuring O_2 diffusion through the hydrogel constructs. (C) Quantified O_2 concentrations above the hydrogels and below the hydrogels at different time points. (D, E) Photographs showing the efficient passage of culture medium through (D) a porous hydrogel and (E) a standard hydrogel. Note the difference in the color of the medium: the photo on the left was taken almost immediately after adding the medium on top, and the photo on the right was taken after 24 h. (F, G) Photographs showing the efficient passage of colored microbeads through (F) a porous hydrogel and (G) a standard hydrogel, each placed on top of piece of filter paper.

emulsion system, when the two aqueous phases used are meticulously selected [41,42]. As such, it has been demonstrated that it was possible to directly write [43] or print [44] an aqueous pattern within another aqueous bath, or produce droplets using microfluidic devices [45–49]. The unique advantage of biocompatibility of the aqueous two-phase emulsion system allows it to be used in the presence of cells without exerting any toxicity otherwise imposed by the organic solvents in conventional emulsions.

To this end, we have recently reported an unprecedented aqueous two-phase emulsion bioink, composed of GelMA as the continuous phase while PEO as the emulsion droplets [21]. We chose GelMA as this cost-effective derivative of gelatin features intrinsic cell instructive moieties, along with on-demand photocrosslinkability [24,50–52]. Similarly, PEO is a biocompatible macromolecule commonly used in tissue engineering applications [53–55]. On crosslinking of the GelMA phase to form a hydrogel matrix, the PEO droplets could be selectively removed by simply soaking the construct in saline or cell culture medium. Importantly, the pore size was readily adjustable within a wide range from approximately 20 μm to about 100 μm, through altering both the concentrations of the polymers and the ratios of the two phases [21]. In addition, it was proven that, the pore size could also be easily controlled by altering the mixing time of the GelMA and the PEO solutions (Fig. 3A and B). When the GelMA phase was fixed at 10 wt% and PEO at 1.6 wt%, as the mixing time was increased from 5 to 10 s and 15 s, the pore size decreased from 105.44 ± 34.7 μm, to 63.9 ± 19.6 μm and 32.5 ± 15.0 μm. From the pore size distribution data (Fig. S1), it could be further observed that as the mixing time was prolonged, the pores became slightly more uniform. A mixing time of 10 s was selected for subsequent experiments. In comparison, a standard GelMA hydrogel possessed only nanometer meshes without any visible micropores under either fluorescence microscopy or scanning electron microcopy (SEM) (Fig. 3C).

We hypothesized that the interconnected micropores in our GelMA hydrogels would accordingly facilitate the transport of gas and nutrients, which is important in promoting wound healing [56,57]. We first investigated into oxygen (O_2) transport across the hydrogel constructs using a customized setup (Fig. 4A and B). Indeed, as revealed in Fig. 4C, the diffusion of O_2 through the porous hydrogel was decently fast; although the level below the hydrogel was low initially at 0 min, it rapidly increased within 1 h, to almost the same level right above the construct undergoing constant O_2 bubbling. In contrast, even after 60 min of active bubbling, the concentration of O_2 remained relatively low at below 15 mg L^{-1}, only 50% of that above the hydrogel. Fluid transport results were similar when comparing the two types of hydrogel constructs. Two sets of experiments were performed in this case. One was a dripping assay, where we proved that culture medium could effectively pass through the porous hydrogel nearly in real time under gravity (Fig. 4D) while the passage of the medium under the same condition

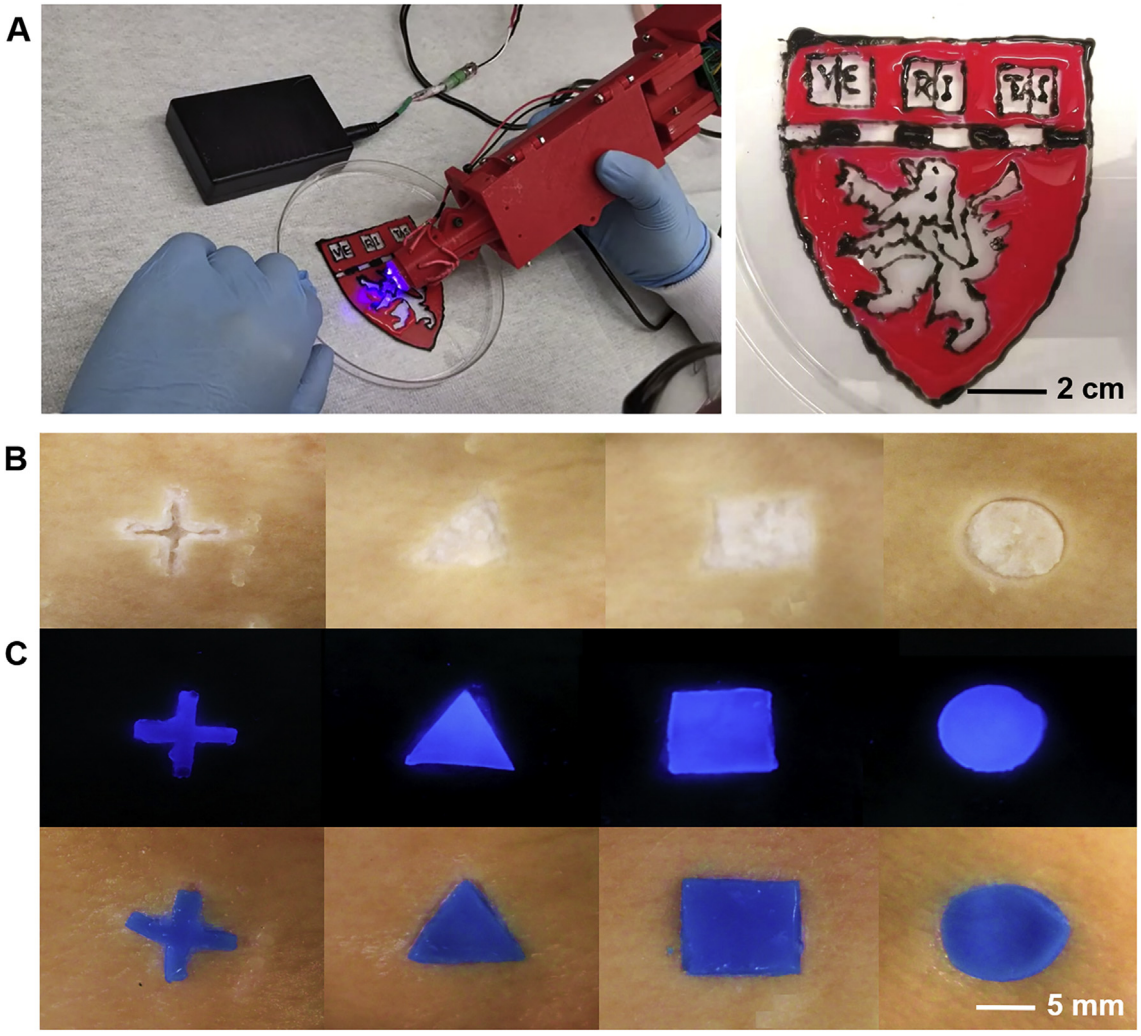

Fig. 5. (A) Handheld bioprinting of a Harvard logo using the pore-forming bioink dyed in different colors. (B, C) Hand-bioprinted pore-forming hydrogel patterns on ex vivo pig skins with artificially created wound shapes. (For interpretation of the references to color in this figure legend, the reader is referred to the Web version of this article.)

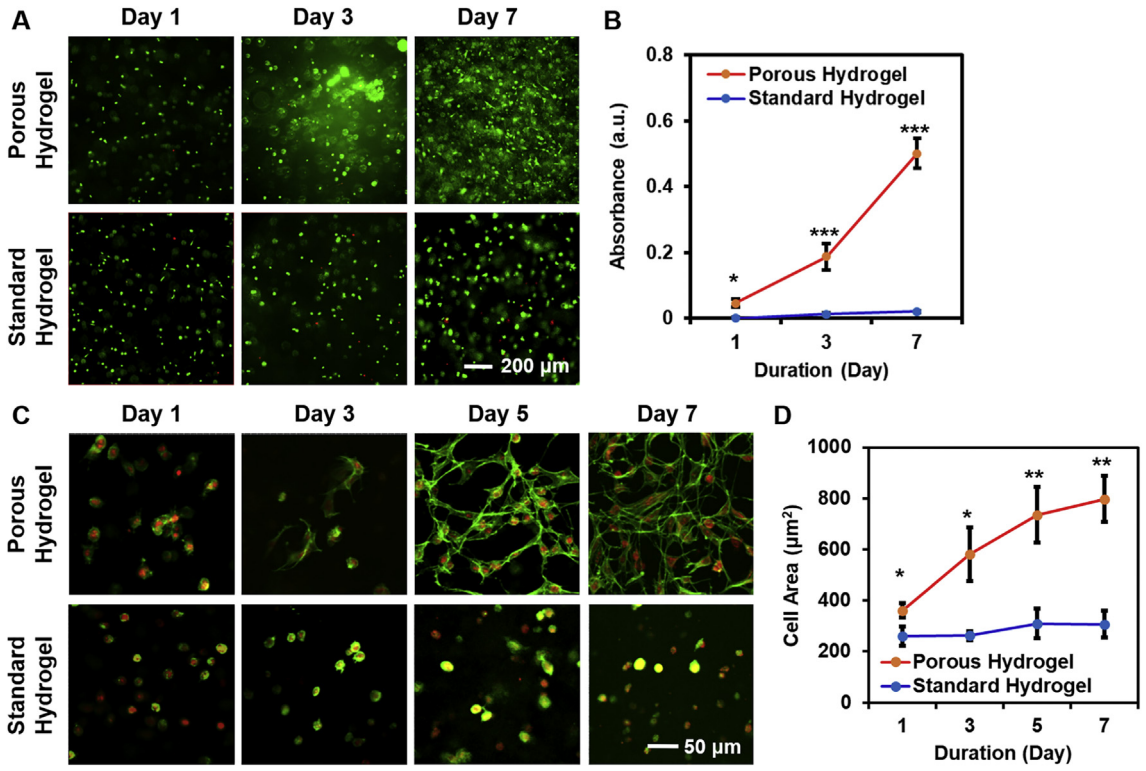

Fig. 6. (A) Live (green)/dead (red) staining of NIH/3T3 fibroblasts in hand-bioprinted porous hydrogel constructs and standard hydrogel constructs at days 1, 3, and 7 of culture. (B) Quantification of cell proliferation in the two types of hydrogel constructs at days 1, 3, and 7 of culture. (C) F-actin (green)/nuclei (red) staining of NIH/3T3 fibroblasts in hand-bioprinted porous hydrogel constructs and standard hydrogel constructs at days 1, 3, 5, and 7 of culture. (D) Quantification of cell spreading areas in the two types of hydrogel constructs at days 1, 3, 5, and 7 of culture. $*p<0.05$, $**p<0.01$, $***p<0.001$ ($n = 3$).

across the standard hydrogel was almost impossible (Fig. 4E). When we placed a drop of colored microbead solution on top of the hydrogel disk, it was also revealed that it could almost immediately wet the porous construct (Fig. 4F), yet the droplet stayed unabsorbed on the standard hydrogel (Fig. 4G). These results were consistent with the dye transport assay, which was previously demonstrated [21].

After the emulsion was formed, it could remain stable for 30–60 min, where the stability would be further promoted by storing at a reduced temperature to allow gelation of the GelMA phase, as needed [21]. This property has enabled its convenient bioprinting using either desktop extrusion bioprinting or digital light processing-based bioprinting, as we previously demonstrated [21]. Yet, the suitability of this pore-forming bioink for handheld bioprinting remains to be investigated. Therefore, we subsequently evaluated the printability of our emulsion bioink using the handheld bioprinter. The bioprinter was low-cost yet showed high performance, with a portable and ergonomic design, allowing conformable holding in hand. The switches made it easy to control the bioprinter operations, such as bioink extrusion ON/OFF, the motor rotation speed (hence the bioink extrusion speed), as well as the syringe replacement (Fig. 2). By loading the pore-forming bioink into the reservoir, we successfully hand-bioprinted a Harvard logo with the help of the UV LED array-enabled in situ photocrosslinking (Fig. 5A). We were able to sequentially write two bioinks, colored in red and black, by simply changing the syringe during the bioprinting process, via the click-openable cover. Moreover, the resolution of the extruded microfibers could be readily adjusted by tuning the motor rotation speed and the nozzle size. Both parameters apparently had positive correlations with the diameters of the bioink fibers extruded (Fig. S2).

To emulate the in vivo bioprinting conditions, we obtained ex vivo porcine skin tissues from the local butcher, where artificially structured wounds were created (Fig. 5B). A unique advantage of intraoperative bioprinting lies in its ability to conformally deposit the wound-dressing material in accordance with the shapes of the injury sites in real time with instant adjustability. To this end, we showed that it was possible to achieve this capability by hand-bioprint our emulsion bioink into the wound areas through moving the printhead with close-to-perfect shape complementarity (Fig. 5C).

As aforementioned, the porosity is instrumental in enhancing cellular behaviors within the bioprinted hydrogel constructs. We have previously shown that, pure GelMA bioinks would not effectively allow cell spreading until their concentrations are lowered down to a sufficiently small value, such as 3 wt% [24]. A dilemma associated with such a low concentration of the GelMA bioink however, is its extremely low mechanical property leading to collapse, to various degrees, of the resulting bioprinted hydrogel structures. Our pore-forming GelMA bioink solved these issues by providing the backbone mechanical support through the relatively high concentrations of GelMA (e.g. 10 wt% used here), as the porosity was supplied by the PEO emulsion droplets that could be subsequently removed via leaching. The viabilities of the NIH/3T3 fibroblasts within the hand-bioprinted constructs were similar across the 7-day culture period (Fig. 6A). Although those in the porous GelMA hydrogel group seemed slightly higher, no major difference could be observed. On the contrary, the cells within the hand-bioprinted porous GelMA constructs indicated significantly faster cell proliferation than those in the standard GelMA hydrogels (Fig. 6B), suggesting that the porous structure could have provided the cells with much more spaces for growth.

We further compared the spreading of the fibroblasts in two types of GelMA hydrogels that were bioprinted using our handheld bioprinter (Fig. 6C and D). Consistent with our previous report [21], the GelMA porous hydrogels noticeably enhanced cell spreading, with cell areas grown from the 361.3 ± 28.2 μm^2 at day 1 to 581.7 ± 105.6, 735.8 ± 110.1, and 798.0 ± 90.2 μm^2 on days 3, 5, and 7, respectively. The standard GelMA hydrogel with only nanoscale meshes, in contrast, did not support cell spreading with cell areas maintaining roughly

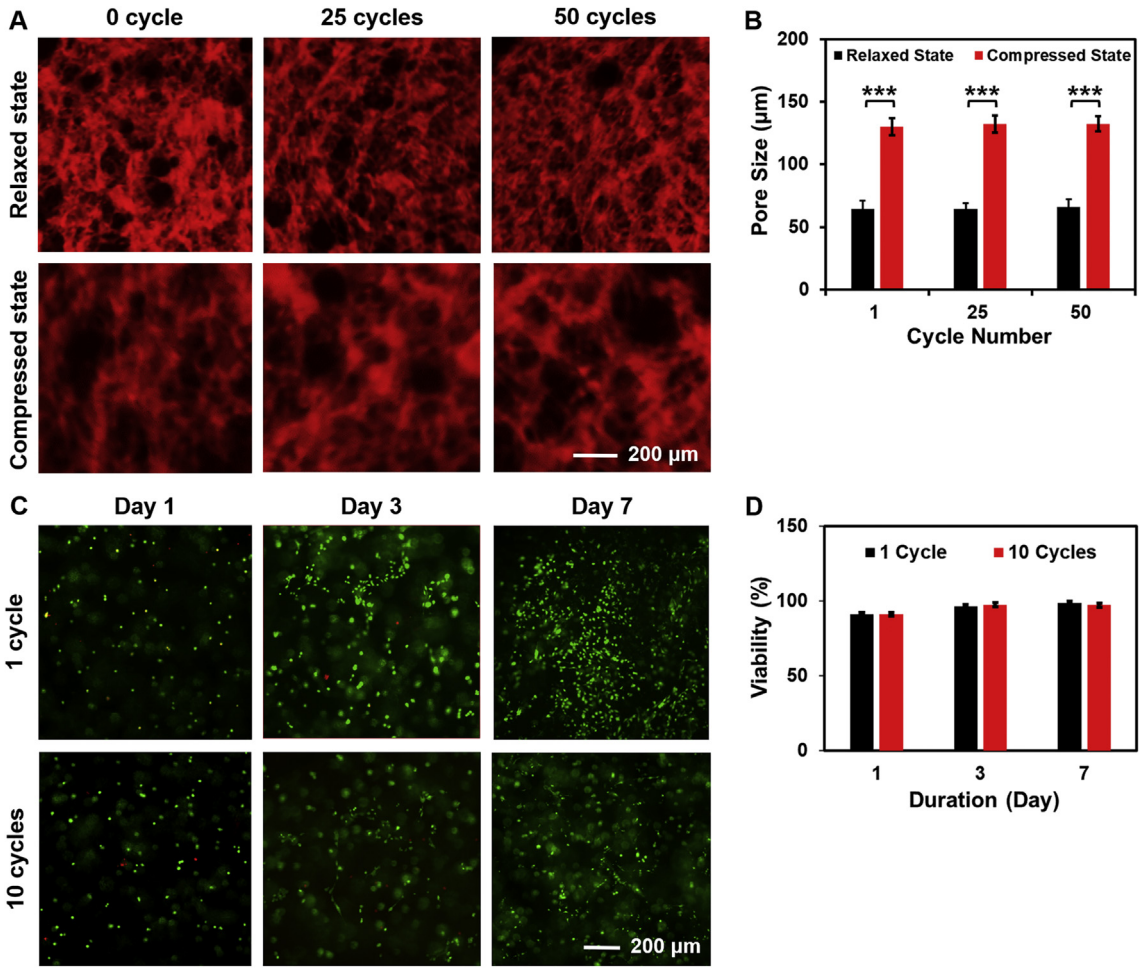

Fig. 7. (A) Confocal fluorescence micrographs showing the morphologies of a hand-bioprinted porous hydrogel construct for up to 50 cycles of compressions, at relaxed and compressed states. (B) Quantification of pore sizes. (C) Live (green)/dead (red) staining of NIH/3T3 fibroblasts in hand-bioprinted porous hydrogel constructs after 1 cycle and 10 cycles of compression at days 1, 3, and 7 of culture. (D) Quantification of cell viability after 1 cycle and 10 cycles of compression at days 1, 3, and 7. ***$p<0.001$ ($n = 3$).

constant from $260.2 \pm 37.5\ \mu m^2$ at day 1 to a merely $306.7 \pm 52.7\ \mu m^2$ by day 7. As vascularization plays a key role in wound healing [58], we have in addition, studied the spreading of HUVECs in the hydrogel constructs. Consistent with the results relating to fibroblasts, the GelMA porous hydrogels promoted the spreading of HUVECs as well, with cell areas increasing from the $353.0 \pm 28.6\ \mu m^2$ at day 1 to $706.7 \pm 69.2\ \mu m^2$ and $1254.7 \pm 107.5\ \mu m^2$ on days 3 and 7 (Fig. S3), respectively. The standard GelMA hydrogel with only nanoscale meshes, in contrast, did not support the spreading of the HUVECs with cell areas maintaining in the range of $346.0 \pm 16.3\ \mu m^2$ at day 1 to $530.0 \pm 46.5\ \mu m^2$ at day 7. These results are important for intraoperative bioprinting, as it is generally desired to have rapid cellularization within the dressing materials to promote rapid wound healing.

Finally, the wound areas on our body may experience constant compressions due to either muscular movements or external forces during daily activities. Therefore, the dressing material should not only facilitate wound healing but also, remain structurally stable while continuing to support normal cellular behaviors when mechanically forced. We hypothesized that the unique microporous structure of our hand-bioprinted pore-forming GelMA hydrogel would readily satisfy these requirements. Interestingly, it was found that the porous GelMA hydrogels possessed favorable elasticity. On compression under a strain of 10%, the pore sizes in the lateral direction were increased, as expected. Nevertheless, on the release of the external force, the hydrogels could completely return to their original shapes with also a regain of their original pore sizes, for up to 50 cycles of continuous compressions tested (Fig. 7A and B). More importantly, after 10 compression cycles, the embedded fibroblasts could still faithfully maintain their viability immediately and after 7 days of culture (Fig. 7C and D), indicating that our unique porous GelMA hydrogels might be an enabling candidate for applications in wound dressing. Of note, the strong elasticity is also seen in other types of porous hydrogels such as the cryogels [59,60]; yet differently, because of the harsh fabrication conditions at subzero degrees, cryogels similar to water/oil emulsions, do not allow cell encapsulation during their production, making them incompatible with in situ bioprinting.

4. Conclusion

In conclusion, we have designed an open-source, portable, and ergonomic handheld bioprinting system. The handheld bioprinter costs only $121, assembled by 3D-printed supports and encasements together with off-the-shelf mechanical and electronic components. To demonstrate its utility in achieving intraoperative bioprinting, we integrated a unique two-phase aqueous emulsion bioink formulation, which was fully biocompatible allowing cell encapsulation during wound dressing. Moreover, the resulting hydrogel dressing, on in situ photocrosslinking, would form interconnected microscale pores that facilitated not only fast transport of fluid and oxygen, but also survival, proliferation, and spreading of the embedded cells. We anticipate widespread applications

of our technology in the future toward rapid and effective in-surgery wound healing potentially in a wound- and patient-specific manner.

Nevertheless, we also see a few limitations of the technology in its current form as reported. For example, multimaterial arrangement may further be incorporated to allow heterogenous dressing [61,62]; the UV LED array may be replaced by that of another wavelength within the visible-light region to avoid any potential photodamage to the skin; and the pore-forming bioink may require further optimizations and characterizations to realize multifunctions such as antibacterial performances.

Funding

This work was supported by funding from the National Institutes of Health (R21EB026175, R01GM134036), the American Heart Association (19TPA34850188), and the Brigham Research Institute.

Data availability

The data sets that support the findings of this study are available from the corresponding authors on reasonable requests. All requests for raw and analyzed data and materials will be promptly reviewed by the Brigham and Women's Hospital to verify whether the requests are subject to any intellectual property or confidentiality obligations. Any data and materials that can be shared will be released via a Material Transfer Agreement.

Author contribution

G. Y, J. Manríquez, D. Wu, J. Zhang, N. Jiang, S. Maharjan, D. H. Hernández Medina: Investigation, Data curation, Formal analysis, Validation, Software, Writing – review & editing.

Y. S. Zhang: Funding acquisition, Project administration, Resources, Supervision, Data curation, Writing – original draft, Writing – review & editing.

Declaration of competing interest

The authors declare that they have no known competing financial interests or personal relationships that could have appeared to influence the work reported in this paper.

Appendix A. Supplementary data

Supplementary data to this article can be found online at https://doi.org/10.1016/j.mtbio.2020.100074.

References

[1] L. Moroni, J.A. Burdick, C. Highley, S.J. Lee, Y. Morimoto, S. Takeuchi, J.J. Yoo, Biofabrication strategies for 3D in vitro models and regenerative medicine, Nature Reviews Materials 3 (5) (2018) 21–37.
[2] S.V. Murphy, P. De Coppi, A. Atala, Opportunities and challenges of translational 3D bioprinting, Nature Biomed Eng (2019) 1–11.
[3] M.A. Heinrich, W. Liu, A. Jimenez, J. Yang, A. Akpek, X. Liu, Q. Pi, X. Mu, N. Hu, R.M. Schiffelers, J. Prakash, J. Xie, Y.S. Zhang, 3D bioprinting: from benches to translational applications, Small 15 (23) (2019) 1805510.
[4] R. Levato, T. Jungst, R.G. Scheuring, T. Blunk, J. Groll, J. Malda, From shape to function: the next step in bioprinting, Adv. Mater. 32 (12) (2020) 1906423.
[5] M.E. Prendergast, J.A. Burdick, Recent advances in enabling technologies in 3D printing for precision medicine, Adv. Mater. 32 (13) (2020) 1902516.
[6] P.D. Dalton, T.B.F. Woodfield, V. Mironov, J. Groll, Advances in hybrid fabrication toward hierarchical tissue constructs, Advanced Science 7 (11) (2020) 1902953.
[7] N. Ashammakhi, S. Ahadian, I. Pountos, S.-K. Hu, N. Tellisi, P. Bandaru, S. Ostrovidov, M.R. Dokmeci, A. Khademhosseini, In situ three-dimensional printing for reparative and regenerative therapy, Biomed, Microdevices 21 (2) (2019) 42.
[8] Y. Wu, D.J. Ravnic, I.T. Ozbolat, Intraoperative bioprinting: repairing tissues and organs in a surgical setting, Trends Biotechnol. 38 (6) (2020) 594–605.
[9] K.W. Binder, W. Zhao, T. Aboushwareb, D. Dice, A. Atala, J.J. Yoo, In situ bioprinting of the skin for burns, J. Am. Coll. Surg. 211 (3) (2010) S76.
[10] A. Skardal, D. Mack, E. Kapetanovic, A. Atala, J.D. Jackson, J. Yoo, S. Soker, Bioprinted amniotic fluid-derived stem cells accelerate healing of large skin wounds, Stem Cells Translational Med. 1 (11) (2012) 792.
[11] A.A. Adib, A. Sheikhi, M. Shahhosseini, A. Simeunović, S. Wu, C.E. Castro, R. Zhao, A. Khademhosseini, D.J. Hoelzle, Direct-write 3D Printing and Characterization of a GelMA-Based Biomaterial for Intracorporeal Tissue Engineering, Biofabrication, 2020.
[12] Y. Chen, J. Zhang, X. Liu, S. Wang, J. Tao, Y. Huang, W. Wu, Y. Li, K. Zhou, X. Wei, Noninvasive in vivo 3D bioprinting, Science Adv. 6 (23) (2020), eaba7406.
[13] A. Urciuolo, I. Poli, L. Brandolino, P. Raffa, V. Scattolini, C. Laterza, G.G. Giobbe, E. Zambaiti, G. Selmin, M. Magnussen, Intravital three-dimensional bioprinting, Nature Biomed. Eng. (2020) 1–15.
[14] N. Hakimi, R. Cheng, L. Leng, M. Sotoudehfar, P.Q. Ba, N. Bakhtyar, S. Amini-Nik, M.G. Jeschke, A. Günther, Handheld skin printer: in situ formation of planar biomaterials and tissues, Lab Chip 18 (10) (2018) 1440–1451.
[15] R.Y. Cheng, G. Eylert, J.-M. Gariepy, S. He, H. Ahmad, Y. Gao, S. Priore, N. Hakimi, M.G. Jeschke, A. Günther, Handheld instrument for wound-conformal delivery of skin precursor sheets improves healing in full-thickness burns, Biofabrication 12 (2) (2020), 025002.
[16] C.S. Russell, A. Mostafavi, J.P. Quint, A.C. Panayi, K. Baldino, T.J. Williams, J.G. Daubendiek, V. Hugo Sánchez, Z. Bonick, M. Trujillo-Miranda, S.R. Shin, O. Pourquie, S. Salehi, I. Sinha, A. Tamayol, In situ printing of adhesive hydrogel scaffolds for the treatment of skeletal muscle injuries, ACS Applied Bio Materials 3 (3) (2020) 1568–1579.
[17] E. Alarcin, T.Y. Lee, S. Karuthedom, M. Mohammadi, M.A. Brennan, D.H. Lee, A. Marrella, J. Zhang, D. Syla, Y.S. Zhang, A. Khademhosseini, H.L. Jang, Injectable shear-thinning hydrogels for delivering osteogenic and angiogenic cells and growth factors, Biomaterials Science 6 (2018) 1604–1615.
[18] P.S. Gungor-Ozkerim, I. Inci, Y.S. Zhang, A. Khademhosseini, M.R. Dokmeci, Bioinks for 3D bioprinting: an overview, Biomaterials Science 6 (5) (2018) 915–946.
[19] J. Groll, J.A. Burdick, D.-W. Cho, B. Derby, M. Gelinsky, S.C. Heilshorn, T. Juengst, J. Malda, V.A. Mironov, K. Nakayama, A definition of bioinks and their distinction from biomaterial inks, Biofabrication 11 (1) (2018), 013001.
[20] L. Shao, Q. Gao, C. Xie, J. Fu, M. Xiang, Y. He, Synchronous 3D bioprinting of large-scale cell-laden constructs with nutrient networks, Adv. Healthcare Mater. (2019) 1901142, n/a(n/a).
[21] G.-L. Ying, N. Jiang, S. Maharjan, Y.-X. Yin, R.-R. Chai, X. Cao, J.-Z. Yang, A.K. Miri, S. Hassan, Y.S. Zhang, Aqueous two-phase emulsion bioink-enabled 3D bioprinting of porous hydrogels, Adv. Mater. 30 (2018) 1805460.
[22] J. Gong, C. Shuurmans, X. Cao, A.M. Van Genderen, W. Li, F. Cheng, J.J. He, A. López, V. Huerta, J. Manríquez, R. Li, H. Li, C. Delavaux, S. Sebastian, H. Wang, J. Xie, M. Yu, R. Masereeuw, T. Vermonden, Y.S. Zhang, Complexation-induced resolution enhancement of 3D-printed hydrogel constructs, Nat. Commun. 11 (2020) 1267.
[23] K. Yue, X. Li, K. Schrobback, A. Sheikhi, N. Annabi, J. Leijten, W. Zhang, Y.S. Zhang, D.W. Hutmacher, T.J. Klein, Structural analysis of photocrosslinkable methacryloyl-modified protein derivatives, Biomaterials 139 (2017) 163–171.
[24] W. Liu, M.A. Heinrich, Y. Zhou, A. Akpek, N. Hu, X. Liu, X. Guan, Z. Zhong, X. Jin, A. Khademhosseini, Y.S. Zhang, Extrusion bioprinting of shear-thinning gelatin methacryloyl bioinks, Adv. Healthcare Mater. 6 (12) (2017) 1601451.
[25] J. Yin, M. Yan, Y. Wang, J. Fu, H. Suo, 3D bioprinting of low-concentration cell-laden gelatin methacrylate (GelMA) bioinks with a two-step cross-linking strategy, ACS Appl. Mater. Interfaces 10 (8) (2018) 6849–6857.
[26] J.P. Armstrong, M. Burke, B.M. Carter, S.A. Davis, A.W. Perriman, 3D bioprinting using a templated porous bioink, Adv. Healthc. Mater. 5 (14) (2016) 1724–1730.
[27] E.S. Place, N.D. Evans, M.M. Stevens, Complexity in biomaterials for tissue engineering, Nat. Mater. 8 (6) (2009) 457–470.
[28] Y.S. Zhang, A. Khademhosseini, Advances in engineering hydrogels, Science 356 (6337) (2017), eaaf3627.
[29] S.-W. Choi, Y. Zhang, S. Thomopoulos, Y. Xia, In vitro mineralization by preosteoblasts in poly(dl-lactide-co-glycolide) inverse opal scaffolds reinforced with hydroxyapatite nanoparticles, Langmuir 26 (14) (2010) 12126–12131.
[30] S.-W. Choi, Y. Zhang, Y. Xia, Three-dimensional scaffolds for tissue engineering: the importance of uniformity in pore size and structure, Langmuir 26 (24) (2010) 19001–19006.
[31] X. Cai, Y. Zhang, L. Li, S.-W. Choi, M.R. MacEwan, J. Yao, C. Kim, Y. Xia, L.V. Wang, Investigation of neovascularization in 3D porous scaffolds in vivo by photoacoustic microscopy and optical coherence tomography, Tissue Eng. C 19 (3) (2013) 196–204.
[32] S.W. Choi, Y. Zhang, M.R. MacEwan, Y.N. Xia, Neovascularization in biodegradable inverse opal scaffolds with uniform and precisely controlled pore sizes, Adv. Healthcare Mater. 2 (1) (2013) 145–154.
[33] Y.S. Zhang, K.P. Regan, Y. Xia, Controlling the pore sizes and related properties of inverse opal scaffolds for tissue engineering applications, Macromol. Rapid Commun. 34 (6) (2013) 485–491.
[34] S.I. Jeong, N.A. Burns, C.A. Bonino, I.K. Kwon, S.A. Khan, E. Alsberg, Improved cell infiltration of highly porous 3D nanofibrous scaffolds formed by combined fiber–fiber charge repulsions and ultra-sonication, J. Mater. Chem. B 2 (46) (2014) 8116–8122.
[35] L.G. Sicchieri, G.E. Crippa, P.T. de Oliveira, M.M. Beloti, A.L. Rosa, Pore size regulates cell and tissue interactions with PLGA–CaP scaffolds used for bone engineering, J. Tissue Eng. Regen. Med. 6 (2) (2011) 155–162.
[36] A. Barbetta, R.J. Carnachan, K.H. Smith, C.-t. Zhao, N.R. Cameron, R. Kataky, M. Hayman, S.A. Przyborski, M. Swan, Porous polymers by emulsion templating, Macromol. Symp. 226 (1) (2005) 203–212.

[37] K.-h. Lin, L.-j. Lai, C.-C. Chang, H. Chen, Assembly of microspheres with polymers by evaporating emulsion droplets, Phys. Rev. 78 (4) (2008), 041408-4.
[38] R.K. Kankala, J. Zhao, C.-G. Liu, X.-J. Song, D.-Y. Yang, K. Zhu, S.-B. Wang, Y.S. Zhang, A.-Z. Chen, Highly porous microcarriers for minimally invasive in situ skeletal muscle cell delivery, Small 15 (25) (2019) 1901397.
[39] I. Cooperstein, M. Layani, S. Magdassi, 3D printing of porous structures by UV-curable O/W emulsion for fabrication of conductive objects, J. Mater. Chem. C 3 (9) (2015) 2040–2044.
[40] N.A. Sears, P.S. Dhavalikar, E.M. Cosgriff-Hernandez, Emulsion inks for 3D printing of high porosity materials, Macromol. Rapid Commun. 37 (16) (2016) 1369–1374.
[41] P.-A. Albertsson, Partitioning in Aqueous Two-phase Systems: an Overview, Wiley, Germany, 1986.
[42] Y. Chao, H.C. Shum, Emerging aqueous two-phase systems: from fundamentals of interfaces to biomedical applications, Chem. Soc. Rev. 49 (1) (2020) 114–142.
[43] H. Tavana, A. Jovic, B. Mosadegh, Q. Lee, X. Liu, K. Luker, G. Luker, S. Weiss, S. Takayama, Nanolitre liquid patterning in aqueous environments for spatially defined reagent delivery to mammalian cells, Nat. Mater. 8 (9) (2009) 736–741.
[44] G. Luo, Y. Yu, Y. Yuan, X. Chen, Z. Liu, T. Kong, Freeform, reconfigurable embedded printing of all-aqueous 3D architectures, Adv. Mater. 31 (49) (2019) 1904631.
[45] Y. Song, A. Sauret, H. Cheung Shum, All-aqueous multiphase microfluidics, Biomicrofluidics 7 (6) (2013), 061301.
[46] K. Zhu, Y. Yu, Y. Cheng, C. Tian, G. Zhao, Y. Zhao, All-aqueous-phase microfluidics for cell encapsulation, ACS Appl. Mater. Interfaces 11 (5) (2019) 4826–4832.
[47] Y. Zou, J. Song, X. You, J. Yao, S. Xie, M. Jin, X. Wang, Z. Yan, G. Zhou, L. Shui, Interfacial complexation induced controllable fabrication of stable polyelectrolyte microcapsules using all-aqueous droplet microfluidics for enzyme release, ACS Appl. Mater. Interfaces 11 (23) (2019) 21227–21238.
[48] T. Watanabe, I. Motohiro, T. Ono, Microfluidic formation of hydrogel microcapsules with a single aqueous core by spontaneous cross-linking in aqueous two-phase system droplets, Langmuir 35 (6) (2019) 2358–2367.
[49] Q. Ma, Y. Song, W. Sun, J. Cao, H. Yuan, X. Wang, Y. Sun, H.C. Shum, Cell-inspired all-aqueous microfluidics: from intracellular liquid–liquid phase separation toward advanced biomaterials, Advanced Science 7 (7) (2020) 1903359.
[50] W. Schuurman, P.A. Levett, M.W. Pot, P.R. van Weeren, W.J.A. Dhert, D.W. Hutmacher, F.P.W. Melchels, T.J. Klein, J. Malda, Gelatin-methacrylamide hydrogels as potential biomaterials for fabrication of tissue-engineered cartilage constructs, Macromol. Biosci. 13 (5) (2013) 551–561.
[51] A.K. Miri, H.G. Hosseinabadi, B. Cecen, S. Hassan, Y.S. Zhang, Permeability mapping of gelatin methacryloyl hydrogels, Acta Biomater. 77 (2018) 38–47.
[52] G. Ying, N. Jiang, C. Yu, Y.S. Zhang, Three-dimensional bioprinting of gelatin methacryloyl (GelMA), Bio-Design. Manufacturing 1 (4) (2018) 215–224.
[53] H. Koo, G.-w. Jin, H. Kang, Y. Lee, H.Y. Nam, H.-s. Jang, J.-S. Park, A new biodegradable crosslinked polyethylene oxide sulfide (PEOS) hydrogel for controlled drug release, Int. J. Pharm. 374 (1–2) (2009) 58–65.
[54] C.A. DeForest, B.D. Polizzotti, K.S. Anseth, Sequential click reactions for synthesizing and patterning three-dimensional cell microenvironments, Nat. Mater. 8 (8) (2009) 659–664.
[55] C.A. DeForest, K.S. Anseth, Cytocompatible click-based hydrogels with dynamically tunable properties through orthogonal photoconjugation and photocleavage reactions, Nat. Chem. 3 (12) (2011) 925–931.
[56] S. Schreml, R.M. Szeimies, L. Prantl, S. Karrer, M. Landthaler, P. Babilas, Oxygen in acute and chronic wound healing, Br. J. Dermatol. 163 (2) (2010) 257–268.
[57] G. Han, R. Ceilley, Chronic wound healing: a review of current management and treatments, Adv. Ther. 34 (3) (2017) 599–610.
[58] M.G. Tonnesen, X. Feng, R.A. Clark, Angiogenesis in wound healing, in: Journal of Investigative Dermatology Symposium Proceedings, Nature Publishing Group, 2000, pp. 40–46.
[59] S.A. Bencherif, R.W. Sands, D. Bhatta, P. Arany, C.S. Verbeke, D.A. Edwards, D.J. Mooney, Injectable preformed scaffolds with shape-memory properties, Proc. Natl. Acad. Sci. U.S.A. 109 (48) (2012) 19590–19595.
[60] S.T. Koshy, T.C. Ferrante, S.A. Lewin, D.J. Mooney, Injectable, porous, and cell-responsive gelatin cryogels, Biomaterials 35 (8) (2014) 2477–2487.
[61] W. Liu, Y.S. Zhang, M.A. Heinrich, F. De Ferrari, H.L. Jang, S.M. Bakht, M.M. Alvarez, J. Yang, Y.-C. Li, G. Trujillo-de Santiago, A.K. Miri, K. Zhu, P. Khoshakhlagh, G. Prakash, H. Cheng, X. Guan, Z. Zhong, J. Ju, G.H. Zhu, X. Jin, S.R. Shin, M.R. Dokmeci, A. Khademhosseini, Rapid continuous multimaterial extrusion bioprinting, Adv. Mater. 29 (2017) 1604630.
[62] M. Rocca, A. Fragasso, W. Liu, M.A. Heinrich, Y.S. Zhang, Embedded multi-material extrusion bioprinting, SLAS Technology 23 (2) (2017) 154–163.